Interface-Sensitive Micro-Imaging Based on X-ray Reflectivity

It is important to understand interfaces since they are omnipresent in nature and control the properties of modern materials. Recently, the authors have succeeded in realizing X-ray reflectivity imaging of heterogeneous interfaces in ultrathin films. To visualize a wide viewing area, the image reconstruction scheme is employed instead of micro-beam scanning. The technique achieves image contrast by using the difference in reflectivity at each in-plane point in the thin film sample. X-ray reflectivity profiles at local positions on the sample can be obtained without using a micro beam, as equivalent information can be extracted from a series of wide X-ray reflection projection datasets collected as a function of grazing angle.

The authors have developed the X-ray reflectivity imaging technique [1-4]. A schematic of the experimental setup at BL-14B is shown in **Fig. 1**. In the experiment, the X-rays were monochromated to 16 keV by a double-crystal Si 111 monochromator having an energy resolution of 10^{-4}. The monochromatic X-rays were collimated to form a thin parallel beam. The primary collimating slit was set at 22.5 m from the wiggler source, to collimate the beam to 1 mm (horizontal, H) × 8 mm (vertical, V). The incident X-ray intensity was monitored throughout the experiment by an ionization chamber (D_0) set 0.45 m behind the primary slit. In front of the entrance window of D_0, a fixed width (100 mm, H) slit was attached to further cut the beam horizontally; thus, the final size of the incident beam was 0.10 mm (H) × 8 mm (V). The sample stage, which was set at 0.45 m downstream from D_0, is based on a high-precision goniometer with an accuracy of 0.001°. A rotational motor is vertically attached to an L-shaped stand fixed on the goniometer to realize in-plane rotation (φ-axis in **Fig. 1**). The samples were vertically mounted using a sample holder. The sample holder was equipped with two manual tilt stages. The parallel beam illuminated around 10 mm [H, the footprint length of the X-rays, is always long enough to cover the silicon substrate size (10 mm)] × 8 mm (V) of the sample surface at grazing-incidence geometry. The reflected X-rays were recorded by an X-ray CCD camera (pixel size 6.45 μm) set 0.30 m on the downstream side of the sample as a one-dimensional projection image, where the imaging conditions are in the near-field regime.

An X-ray reflectivity imaging example of buried heterogeneous interfaces is shown in **Fig. 2**. Here, a patterned ultrathin film was studied by the imaging approach. The sample was fabricated on a pre-cleaned silicon substrate by an Eiko DID-5A magnetron sputtering system. Under the top uniform Ti layer the heterogeneous layer consists of two groups of thin films, as shown in panel **a**: (i) Au thin films including the top-left polygon and bottom-right rectangle with different thicknesses; (ii) Ni thin films consisting of the bottom-left thick rectangle, top-right triangle and center-right thin bar with different thicknesses. Panel **b** is an X-ray reflectivity sinogram of the sample at a specific incidence angle corresponding to the wavevector transfer $Q_z = 4\pi \sin\theta/\lambda = 0.0502$ Å^{-1} (θ: the grazing incidence angle in **Fig. 1**, λ: X-ray wavelength), where obvious sinusoidal patterns are observed.

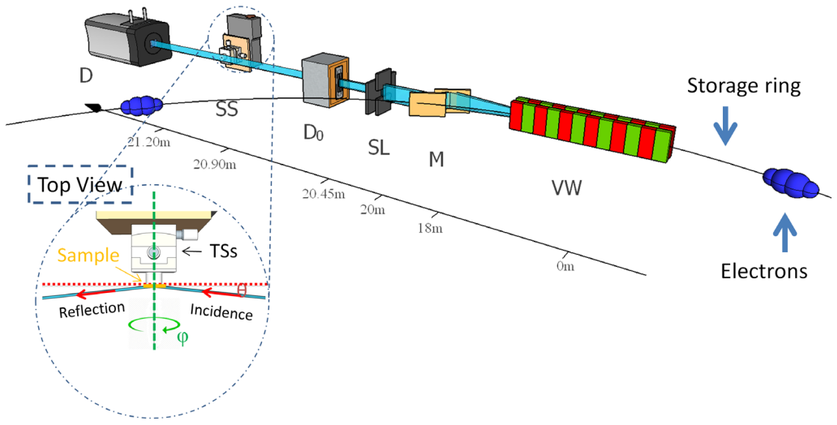

Figure 1: Schematic of the X-ray reflectivity imaging experimental set-up. VW: BL-14 vertical wiggler; M: monochromator; SL: 2D slit; D_0: ionization chamber, with a horizontal slit (0.05 mm, H); SS: sample stage on a goniometer; D: X-ray CCD camera. Inset is the enlarged image of SS from the top view: TSs: tilting stages. Reprinted, with permission, from reference [1].

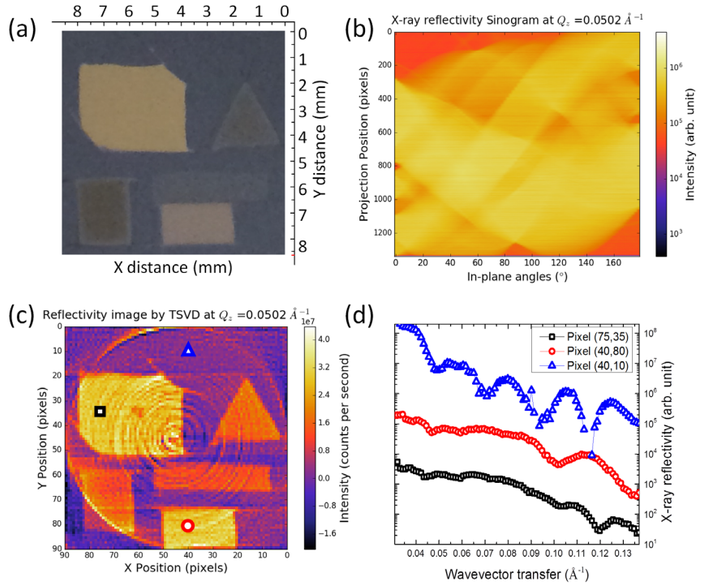

Figure 2: Typical X-ray reflectivity imaging data. **(a)** An optical image of a heterogeneous patterned (Au and Ni) ultrathin film sample before coating with a Ti uniform layer. **(b)** An X-ray reflectivity sinogram of the sample at Q_z = 0.0502 Å^{-1}. **(c)** A reconstructed X-ray reflectivity image of the sample at Q_z = 0.0502 Å^{-1}. **(d)** Three selected μXR profiles at local positions [as indicated by the same symbols in panel **(c)**] of the sample extracted from reconstructed X-ray reflectivity images. Reprinted, with permission, from reference [2].

The 1338 pixels are equally binned into 90 pixels (pixel length: 96 μm, 96 μm × 90 = 8.6 mm). The algebraic imaging reconstruction approach is employed to quantitatively reconstruct the X-ray reflectivity image. Panel **c** presents the corresponding reconstructed X-ray reflectivity image of the sample at Q_z = 0.0502 Å^{-1}. Although the sample is buried by the top Ti layer, the Au and Ni patterns are clearly observed by X-ray reflectivity imaging. At this wavevector transfer, the Au patterns produce higher reflectivity than the Ni patterns, thus giving a contrast between the patterns of the two different materials.

By scanning grazing angles, a series of X-ray reflectivity images sampled equally over a range of wavevector transfers is collected, thus μXR, which is the X-ray reflectivity profile at every micro-sized pixel, can be extracted. Panel **d** shows three selected μXR profiles. The pixel [40, 10] contains only a uniform Ti layer. The μXR profile confirms this point by displaying a sharp drop at Q_z = 0.042 Å^{-1} and equal-period interference fringes. At pixels [40, 80] and [75, 35], the μXR has an intensity drop around Q_z = 0.042 Å^{-1} and shallow oscillations below Q_z = 0.080 Å^{-1}. Beyond Q_z = 0.080 Å^{-1}, the μXR profile drops sharply and experiences deep oscillations. The two μXR profiles of Au patterns show different oscillation periods beyond Q_z = 0.080 Å^{-1}, indicating the different thicknesses of the patterns.

In the present research, X-ray reflectivity imaging was achieved by combining φ-scan and measurement of the 1D intensity profile of reflection projection. It has been demonstrated that the technique yields interface-sensitive images of ultrathin film samples. The new technique enables the non-destructive study of interfaces.

REFERENCES

[1] J. Jiang, K. Hirano and K. Sakurai, *J. Appl. Phys.* **120**, 115301 (2016).
[2] J. Jiang, K. Hirano and K. Sakurai, *J. Appl. Crystallogr.* **50**, 712 (2017) .
[3] K. Sakurai and J. Jiang, *J. Surf. Sci. Soc. Japan.* (2017) (in Japanese language, in press).
[4] J. Jiang and K. Sakurai, *Rev. Sci. Instrum.* **87**, 93709 (2016).

BEAMLINE

BL-14B

J. Jiang[1, 2], K. Hirano[3] and K. Sakurai[2, 1] ([1]Univ. of Tsukuba, [2] NIMS, [3]KEK-IMSS-PF)

A Novel Strategy to Reveal Latent Liver Abnormalities in Human Embryonic Stages from a Large Embryo Collection

The cause of spontaneous abortion of normal conceptuses remains unknown in most embryos because of the difficulty of diagnosing too small embryos. We aimed to reveal latent liver abnormalities using novel phase-contrast radiographic computed tomography (PXCT). Embryos with liver volumes ≥ 2 SD above or below the mean for the stage of development were screened from 1156 MR images from the Kyoto Collection. Selected embryos were further analyzed by using PXCT. Liver abnormality was detected in 9 embryos by our protocol. Most of such liver abnormality embryos do not survive, as liver function becomes essential.

The cause of spontaneous abortion of normal conceptuses remains unknown in most embryos [1] because of the difficulty of obtaining appropriate embryo materials as well as diagnosing internal abnormalities in very small embryos. The crown-rump length of an embryo is ranging 23 to 32 mm during the embryonic period by Carnegie stage (CS) 23 (about 56–60 days after fertilization) [2], by which stage all primordia of the organs are already provided.

Many factors are involved in spontaneous abortion, not only the embryonic factor itself but also maternal health and the intrauterine environment affected by unspecified modulators. Such complicated factors distract attention from the laborious inspection of embryos, especially when embryos are externally normal.

More than 40,000 embryo and fetal specimens have been collected in the Kyoto Collection since 1961 for revealing the mechanism of congenital anomalies [3]. An MRI database of approximately 1200 well-preserved human embryos, diagnosed as externally normal, was acquired in 2000–2005 (the Kyoto embryo visualizing project) [4] to observe a number of normal human embryos. The database has proven to be useful for research purposes and as a teaching material [5].

Although the MRI database includes only externally normal embryo specimens, whether the internal organs were also normal cannot be guaranteed. Considering that the cumulative intrauterine mortality rate in normal conceptuses was estimated at 18% [1], the MRI database includes embryos that have potential abnormalities that would have led to spontaneous abortion. Thus, detailed observation of the internal organs of embryo specimens from the database may provide clues to spontaneous abortion in the embryonic and fetal periods. In this connection, we aimed to determine the latent abnormalities that may cause spontaneous abortion by using the MRI database and novel phase-contrast radiographic computed tomography (PXCT).

The MRI database was screened by using the volume of the liver as the target organ. Embryos with liver volumes ≥ 2 SD above or below the mean for the stage of development were selected. Embryos with potentially abnormal livers were further analyzed by using PXCT. The PXCT data provide a resolution of ≥ 18 μm/pixel, which enabled highly sensitive measurement, approximately > 1000 times more sensitive than the conventional radiographic method using absorption contrast [6].

Liver abnormality was detected in 9 embryos after the procedure of our protocol (Fig. 1), which consisted of hepatic agenesis (2 embryos), hepatic hypogenesis (4), liver lobe defect (1), involvement of the liver to the thoracic cavity by diaphragm herniation (1), and other (1). Three embryos had only liver abnormalities and 6 exhibited complications in other organs. The prevalence of liver malformations in CS18 and CS21 in the intrauterine population of externally normal embryos is approximately 1.7%. Most of such liver abnormality embryos do not survive, as liver function becomes essential during development [7].

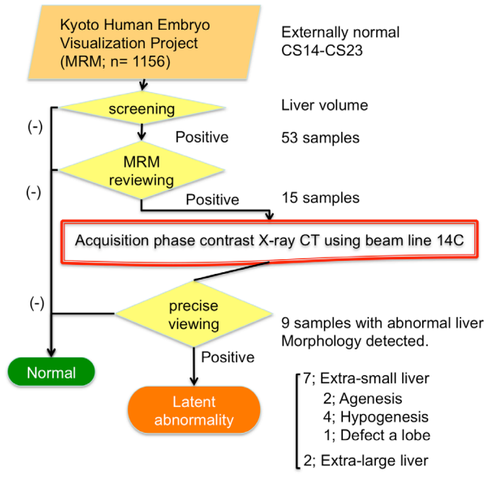

Figure 1: Protocol for detecting latent abnormal embryos that may result in spontaneous abortion.

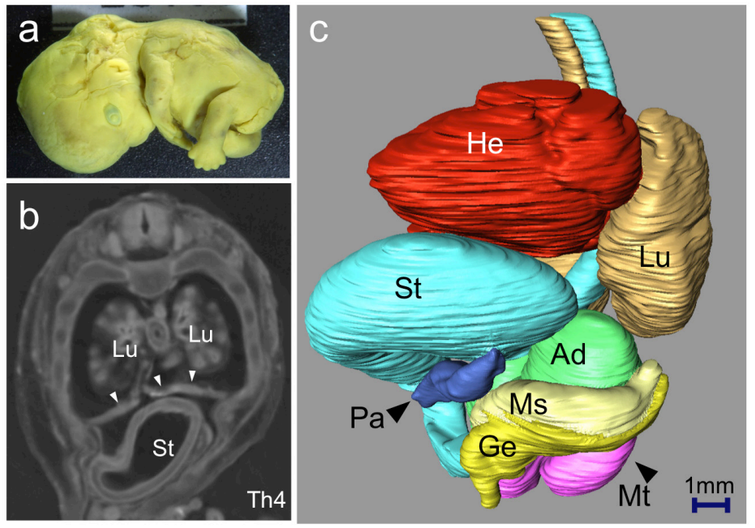

Figure 2: Representative embryos with liver abnormality (liver agenesis).
a External view of the embryo at CS21, which shows no obvious external abnormality. **b** Phase-contrast X-ray computed tomography (PXCT) transverse sections at the level of Th4. No liver (Li) was detected in the plane sections, while the stomach (St) was observed in the midsagittal transverse sections at Th4. The diaphragm is indicated by arrow heads. Lung (Lu). **c** Left anterior oblique view of the three-dimensional (3-D) PXCT reconstruction of the embryo using Amira software (Visage Imaging, Berlin, Germany), demonstrating the locations of all intrathoracic, retroperitoneal, and intra-abdominal organs.
The findings of note were as follows: agenesis of the liver; the stomach was deviated ventrally and cranially; the pancreas (Pa) was deviated ventrally; and the right mesonephros (Ms) and genital ridge (Ge) were absent. Adrenal gland (Ad), metanephros (Mt), and heart (He).

A representative embryo with liver agenesis is shown in Fig. 2. The size and gestational age were within the normal range for the embryo at CS 21. Obvious damage to, or anomalies of, the external forms were not present (Fig. 2a). The liver at CS21 usually occupies a large space in the abdominal cavity, which has a smooth surface due to the contact between the cranial surface and the diaphragm, and between the ventral surface and the abdominal wall [7]. In the present embryos, the liver was not detected in any of the serial plane sections (Fig. 2b). The locations of all intrathoracic, retroperitoneal, and intra-abdominal organs were reconstructed in three dimensions (Fig. 2c). The absence of the liver had affected the locations of the other internal organs, especially the stomach, duodenum, and pancreas. The stomach was observed on the midsagittal line in the Th4 transverse sections, indicating that the stomach had deviated cranially and ventrally. The diaphragm was apparent in these sections.

The present study demonstrates that PXCT may be considered a powerful tool for visualization of internal structures of embryos, and for the detection of novel abnormalities during the embryonic period, without the need for histological analysis. The non-invasive and non-destructive properties of the technique are important for analysis of scarce specimens, such as human embryos. The present study is the first step toward elucidating the latent abnormalities that result in spontaneous abortion in externally normal embryos [8].

REFERENCES

[1] K. Shiota, *Congenital Anomalies* **31**, 67 (1991).
[2] R. O'Rahilly and F. Müller, *Developmental stages in human embryos: including a revision of Streeter's" horizons" and a survey of the Carnegie Collection*, (Carnegie Institution of Washington Publishing. 1987).
[3] H. Nishimura, K. Takano, T. Tanimura and M. Yasuda, *Teratology* **1**, 281 (1968).
[4] K. Shiota, S. Yamada, T. Nakatsu-Komatsu, C. Uwabe, K. Kose, Y. Matsuda, T. Haishi, S. Mizuta and T. Matsuda, *Am J Med Genet A* **143A**, 3121 (2007).
[5] T. Takakuwa, *Antat Rec* (2017), in press.
[6] A. Yoneyama, S. Yamada and T. Takeda, *Fine Biomedical Imaging Using X-Ray Phase-Sensitive Technique,* eds. G. D. Gargiulo and A. McEwan, *Advanced Biomedical Engineering* **107** (2011).
[7] A. Hirose, T. Nakashima, S. Yamada, C. Uwabe, K. Kose and T. Takakuwa, *Anat Rec* **295**, 51 (2012).
[8] T. Kanahashi, S. Yamada, M. Tanaka, A. Hirose, C. Uwabe, K. Kose, A. Yoneyama, T. Takeda and T. Takakuwa, *Anat Rec* **299**, 8 (2016).

BEAMLINE

BL-14C

T. Takakuwa (Kyoto Univ.)